




REGULAR ARTICLE

Ag Nanoparticles Concentration Impact on Plasmon-Enhanced Fluorescence of Pyrene in Solution and Nanocomposite Thin Film

P.V. Demydov^{1,*} , A.M. Lopatynskiy^{1,2}, V.V. Kuznietsov¹, V.K. Lytvyn¹, M.M. Khutko¹, V.I. Chegel^{1,2}

¹ V. Lashkaryov Institute of Semiconductor Physics, National Academy of Sciences of Ukraine, 03028 Kyiv, Ukraine

² Educational and Scientific Institute of High Technologies, Taras Shevchenko National University of Kyiv, 01601 Kyiv, Ukraine

(Received 16 October 2025; revised manuscript received 17 December 2025; published online 19 December 2025)

This work investigates the influence of silver nanoparticles (AgNPs) concentration on the plasmon-enhanced fluorescence (PEF) of pyrene molecules in solutions and embedded in nanocomposite polymer-based thin films. By employing numerical electromagnetic modeling to estimate AgNPs size and nanoparticle-fluorophore distance influence on PEF efficiency, and systematically varying the AgNPs concentration in experimental studies, we examine how their localized surface plasmon resonance modulates the fluorescence intensity and spectral characteristics of pyrene in aqueous solutions and AgNPs/pyrene/polyvinylpyrrolidone thin films fabricated via spin-coating. Our results demonstrate a non-linear relationship between AgNPs concentration and fluorescence intensity of pyrene, with an optimal pyrene-AgNPs volume ratios of 1:2 and 1:1 that maximize fluorescence enhancement factor for solution (~ 1.8 times) and nanocomposite thin film (~ 2.1 times), respectively. The role of polymer matrix for maximizing the PEF effect and preventing fluorescence quenching is discussed. These findings provide insights into the tunability of PEF in hybrid nanostructures and highlight the importance of nanoparticle concentration factor in designing efficient plasmonic fluorescence systems for sensing and photonic applications.

Keywords: Silver nanostructures, Pyrene, Plasmon-enhanced fluorescence, Localized surface plasmon resonance, Finite element method, Nanocomposite

DOI: [10.21272/jnep.17\(6\).06010](https://doi.org/10.21272/jnep.17(6).06010)

PACS numbers: 33.50. – j, 78.67.Sc, 73.20.Mf, 81.07.Bc, 82.35.Np

1. INTRODUCTION

Noble metal nanoparticles, particularly silver (Ag) and gold (Au), have gained significant interest in nanophotonics and sensing applications due to their ability to support localized surface plasmon resonance (LSPR) – coherent oscillations of electrons excited by incident light [1-3]. These LSPR modes exhibit strong electromagnetic near field enhancement, which can significantly modify the photophysical properties of nearby fluorophores [4, 5]. This phenomenon is a basis for plasmon-enhanced fluorescence (PEF), occurring when the presence of metallic nanostructures leads to the increased fluorescence intensity, quantum yield, and altered emission dynamics of molecular emitters [6-9].

Among various organic luminophores, pyrene has emerged as a model fluorophore for studies of molecular photophysics, excimer formation, and environment-sensitive fluorescence [10-12]. Its relatively high quantum yield, spectral overlap with the LSPR band of Ag nanoparticles (AgNPs), and well-known aggregation-dependent behavior make pyrene an ideal candidate for exploring plasmon-fluorophore interactions [13, 14]. The integration of AgNPs

and pyrene molecules into nanocomposite thin films offers a platform for probing and tuning plasmon-fluorophore coupling. In such systems, key parameters including nanoparticle size, shape, distribution, and, most importantly, concentration, define the extent of plasmonic enhancement or quenching [15]. At very low concentrations, non-radiative energy transfer can lead to fluorescence quenching. However, at some ratio between nanoparticles and fluorophore concentrations, the near-field enhancement dominates, typically resulting in fluorescence amplification. Finally, at higher nanoparticles concentrations, increased scattering, reabsorption, and non-radiative energy transfer processes may again lead to fluorescence quenching or spectral distortion [16, 17].

Understanding the concentration-dependent behavior of AgNPs in these composite films is essential for the rational design of plasmonic sensors, light-emitting devices, and fluorescence-based imaging platforms. While previous works have extensively examined distance-dependent and spectral overlap PEF effects [18, 19], as well as specifics of plasmon-enhanced monomer and excimer fluorescence of pyrene and its derivatives [20, 21], the systematic study of nanoparticle

* Correspondence e-mail: vodimed@ukr.net



concentration effects in pyrene-containing nanocomposite films remains relatively underexplored.

In this work, we investigate the influence of AgNPs concentration on the fluorescence emission of pyrene in solution and embedded in a nanocomposite thin film matrix based on polyvinylpyrrolidone. Using spectroscopic analysis and electromagnetic modeling, we evaluate the dual role of AgNPs as both enhancers and quenchers of pyrene fluorescence. The obtained results provide new insights into the optimization of plasmonic nanostructures and their nanocomposites with fluorophores used in hybrid systems for photonic and sensing applications.

2. MATERIALS AND METHODS

2.1 Materials

All chemicals were purchased from Sigma-Aldrich and used as received. For the synthesis of AgNPs, silver nitrate (product no. S6506), sodium citrate tribasic dihydrate (product no. 71402), sodium borohydride (product no. 452882), and hydroxylamine hydrochloride (product no. 159417) were used. As a fluorophore, pyrene (puriss. p.a., for fluorescence, $\geq 99.0\%$, product no. 82648) was used. As a polymer for the composite thin film matrix, polyvinylpyrrolidone (PVP) (average mol wt 40,000, product no. PVP40) was used. Ultrapure deionized water (type I, $R = 18.2 \text{ M}\Omega \text{ cm}$) from the water purification system Adrona B30 Bio was used for the preparation of the aqueous solutions. 2-Propanol (IPA) (product no. 34863) was used to dissolve pyrene while preparing aqueous solutions to the desired concentration.

2.2 Sample Preparation

2.2.1. Synthesis of AgNPs

The two-stage protocol for the synthesis of colloidal AgNPs in an aqueous solution has been previously reported by our group elsewhere [22]. Initially, silver nitrate was reduced using sodium borohydride in the presence of sodium citrate to produce seed nanoparticles ($\sim 4 \text{ nm}$ size). Their size was further increased to $\sim 20 \text{ nm}$ by adding hydroxylamine hydrochloride and silver nitrate. The resulting colloidal solution contained stable spherical nanoparticles with a characteristic yellow color.

2.2.2. Preparation of Pyrene-AgNPs Solutions

Solutions with different pyrene-AgNPs volume ratios were prepared by mixing $100 \mu\text{l}$ of 1 mg/ml pyrene solution in IPA and $0\text{--}800 \mu\text{l}$ of AgNPs. To keep the same conditions across all samples, we kept the total volume at 1 ml by adding water for the rest of volume.

2.2.3. Preparation of Solutions for the Nanocomposite Matrix

$50 \mu\text{l}$ of 1 mg/ml pyrene solution in IPA was added to $100 \mu\text{l}$ of $4 \text{ wt}\%$ PVP solution prepared in a $1:1$ IPA/water medium and sonicated to achieve uniform

dispersion of pyrene for better distribution within the thin film. After that, different volumes of colloidal solution of AgNPs in the range of $0\text{--}50 \mu\text{l}$ were added and a necessary volume of IPA or water was added to keep the total volume at $200 \mu\text{l}$. When excited with a light wavelength of 365 nm , prepared solutions exhibited blue fluorescence emission with a variable intensity depending on the solution composition (Fig. 1a).

2.2.4. Deposition of Nanocomposite Thin Films

The composite mixtures prepared as described in subsection 2.2.3 were deposited onto glass substrates using spin coating at $700\text{--}2000 \text{ rpm}$ for $60\text{--}80 \text{ s}$, resulting in nanocomposite thin films exhibiting blue fluorescence emission under 365 nm excitation (Fig. 1b). The most homogeneous films were achieved while spincoated at 1100 rpm for 80 s . The solution was deposited drop by drop when the substrate was already spinning. In the initial stages, thermal annealing of the resulting sample was also performed in an attempt to improve the film structure, but this step was later found to be detrimental, as pyrene degraded and lost its fluorescent properties at annealing temperatures above $70 \text{ }^\circ\text{C}$.

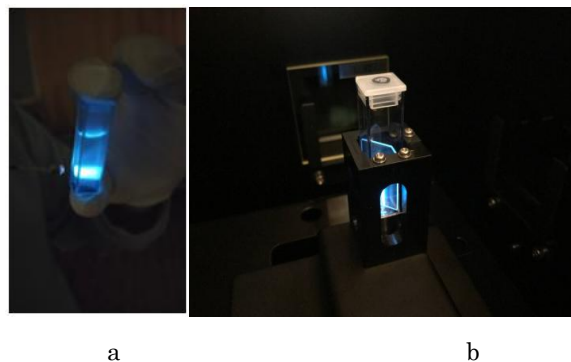


Fig. 1 – Photographs of plasmon-enhanced fluorescence emission of pyrene in the presence of AgNPs in (a) colloidal solution and (b) nanocomposite thin film. Excitation light wavelength is 365 nm

2.3 Fluorescence Measurements

Spectral fluorescence measurements were performed using a RF-6000 spectrofluorophotometer (Shimadzu, Japan) in the spectral range of 365 nm (excitation) and $400\text{--}600 \text{ nm}$ (emission) from both the colloidal solutions of AgNPs containing pyrene and PVP-based nanocomposite thin films with embedded AgNPs and pyrene on glass substrates. Samples were contained in spectrophotometric polystyrene macro cuvettes (Sarstedt 67.754) and deionized water or clear glass substrate were used as reference samples.

2.4 Computer Modeling

To investigate the optimal parameters of nanostructures in terms of PEF, namely, their size, material, and distance between the fluorophore and the

nanoparticle, numerical simulations were performed in the COMSOL Multiphysics environment using the finite element method (FEM). The model was based on a system consisting of a point dipole emitter representing the fluorophore molecule and a spherical metal nanoparticle placed in a dielectric medium. The structure of the model is shown in Fig. 2a: the yellow sphere represents the nanoparticle, the black dot represents the fluorophore, the green area is the dielectric medium, and the blue shell is the perfectly matched layer, which ensures proper electromagnetic wave attenuation at the simulation domain boundaries. An external electromagnetic field was propagating along the X-axis with an initial electric field strength of $E_x = 1$ V/m. The corresponding finite element mesh used for the numerical solution of the problem is shown in Fig. 2b. The model allowed performing simulations of the electromagnetic field distribution in a nanoparticle-fluorophore system depending on the light wavelength and system parameters, thus providing means for the optimization of electric field strength at the fluorophore location, which is known to be directly related to the PEF efficiency [4, 23].

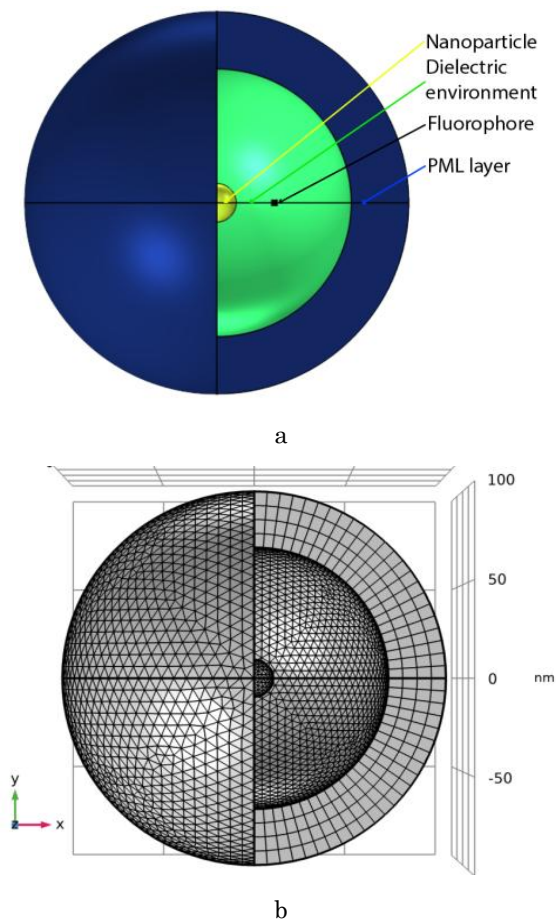


Fig. 2 – (a) Geometry of the model and (b) mesh refinement of the simulation domain.

3. RESULTS AND DISCUSSION

3.1 Computer Modeling of Electromagnetic Field in a Nanoparticle-Fluorophore System

FEM simulations were performed as described in subsection 2.4 for spherical Au and Ag nanoparticles of different size and a point dipole emitter representing a pyrene molecule. Initially, the interaction between a point dipole and a spherical Au nanoparticle with a radius of 10 nm was modeled at the radiation wavelength corresponding to the LSPR wavelength for the given nanoparticle (550 nm). The distance from the surface of the nanoparticle to the dipole position was the variable parameter. Simulation results presented in Fig. 3 show that the electric field strength enhancement is maximum and reaches about 100 at a dipole-to-surface distance of 5 nm. At a distance of 10 nm, field strength enhancement decreases to approximately 40. At a distance of 20 nm and more, the enhancement value further levels off and equals around 20-30 with a maximum at the center of the dipole.

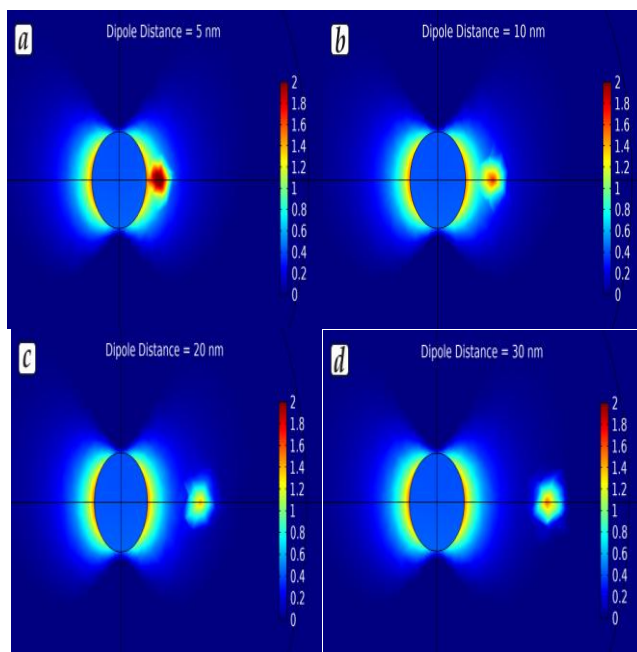


Fig. 3 – Distribution of electric field strength enhancement near a spherical Au nanoparticle with a radius of 10 nm and an adjacent point dipole emitter for various dipole-to-surface distances: a) 5 nm, b) 10 nm, c) 20 nm, d) 30 nm. A logarithmic color scale is used

An analysis of the interaction between a spherical Au nanoparticle and a point dipole depending on the nanoparticle radius, which varied from 10 to 40 nm with a step of 10 nm, was also conducted (Fig. 4). In all cases, the dipole was placed at a distance of 5 nm from the surface of the nanoparticle, allowing evaluation of the influence of the nanostructure geometrical parameters on the local electric field enhancement. As shown in Fig. 4, the highest field enhancement is achieved for the nanoparticle radius of 10 nm, which the radiation

wavelength corresponds to the LSPR wavelength for. Namely, for a nanoparticle radius of 10 nm, the field strength enhancement reaches about 100; for a nanoparticle radius of 20 nm, the maximum field strength enhancement decreases to approximately 30; for a radius of 30 and 40 nm, the peak field strength enhancement is about 50. This result is in agreement with the LSPR wavelength dependence on the nanoparticle size [24] and spectral distribution of the LSPR-induced local electric field enhancement [25].

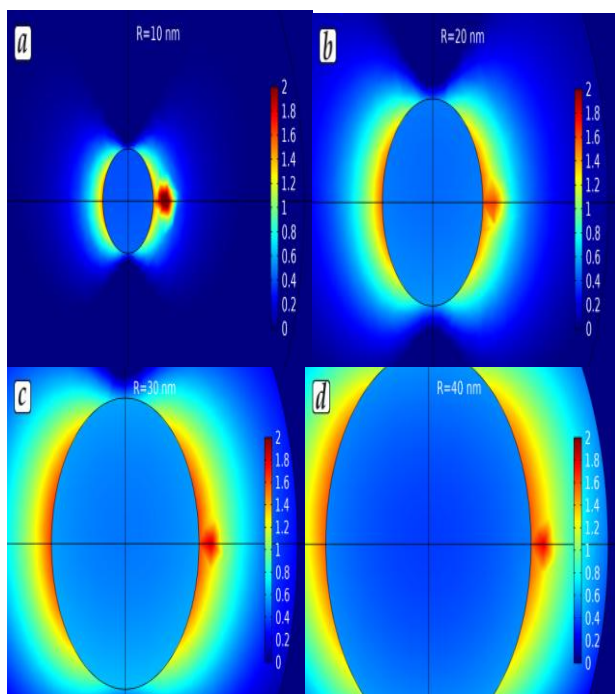


Fig. 4 – Distribution of electric field strength enhancement near a spherical Au nanoparticle with a radius of a) 10 nm, b) 20 nm, c) 30 nm, d) 40 nm and an adjacent point dipole emitter located at a dipole-to-surface distance of 5 nm. A logarithmic color scale is used

The influence of the nanoparticle material on the local electric field strength was studied by simulations performed for spherical silver and gold nanoparticles with a radius of 10 nm at different radiation wavelengths representing the fluorophore excitation and emission (Fig. 5). The field strength was averaged across a plane of 5 nm along the X-axis and 6 nm along the Y-axis in order to smooth the inhomogeneous field distribution near the point dipole location. Simulation results show that the average electric field strength enhancement during the interaction of a fluorophore molecule and a spherical plasmonic nanostructure with a radius of 10 nm under the conditions of the plasmon-enhanced fluorescence phenomenon depends on the material of the nanostructure and is the largest for silver nanostructures in the near UV (360 – 380 nm) and blue (470 nm) spectral ranges and for gold nanostructures in the red spectral range (660 nm).

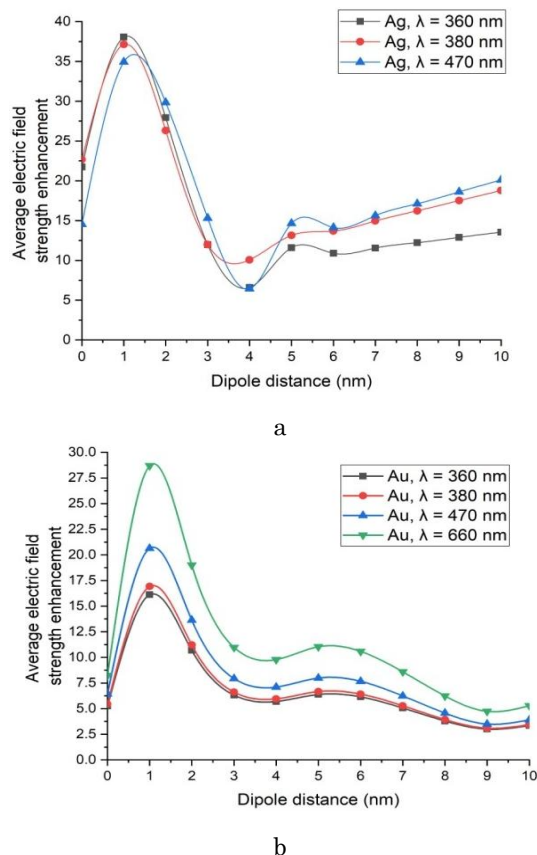


Fig. 5 – Dependences of average electric field strength enhancement on the dipole-to-surface distance for spherical a) silver and b) gold nanoparticles with a radius of 10 nm at different radiation wavelengths

3.2 Fluorescence Measurements of Pyrene-AgNPs Solutions with Different AgNPs Concentration

According to modeling results for the 10-nm-radius AgNPs obtained in subsection 3.1 that predict their higher PEF efficiency in the near UV and blue spectral ranges relevant for pyrene fluorescence in comparison to the nanoparticles of other material and size, spherical AgNPs with a diameter of 10–20 nm were selected and synthesized as described in subsection 2.2.1 for the use in experimental studies. Solutions with different pyrene-AgNPs volume ratios were prepared as described in subsection 2.2.2 and their fluorescence spectra were measured (Fig. 6). Pure pyrene solution showed 2.3 times higher fluorescence intensity than 2:1 pyrene-AgNPs solution and exhibited up to ~1.8 times lower intensity than solutions with other pyrene-AgNPs ratios (1:1-1:8). Therefore, the PEF effect can be achieved in a broad range of the pyrene-AgNPs volume ratio in solution (1:1-1:8), except for a 2:1 ratio when fluorescence quenching occurs, with the ratio of 1:1 showing one of the highest intensities with less material spent. Consequently, we chose the pyrene-AgNPs volume ratio of 1:1 as an upper limit for the further study involving nanocomposite thin films.

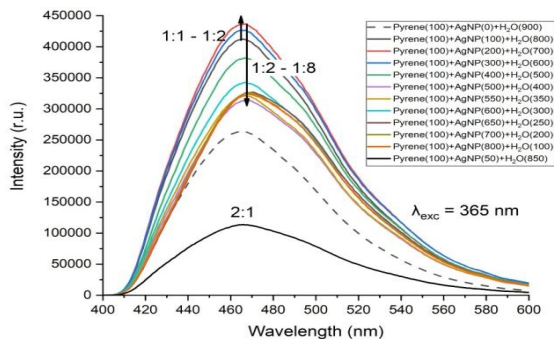


Fig. 6 – Fluorescence spectra of solutions containing pure pyrene (dashed line) and different pyrene-AgNPs volume ratios in the range of 2:1 – 1:8 (solid lines). Volumes of solution components in microliters are shown in the legend

The dependence of peak fluorescence intensity at 465 nm on the AgNPs volume in solution derived from the measured fluorescence spectra was plotted and approximated with a 4th order polynomial fit in Fig. 7 to further investigate the trend of fluorescence intensity changes for the different pyrene-AgNPs volume ratios. It is evident that the highest fluorescence intensity (~ 1.8 times higher than pure pyrene) is achieved for the AgNPs volume of 200 μl (i.e. pyrene-AgNPs ratio of 1:2) and further AgNPs concentration increase results in a gradual fluorescence intensity decrease with a plateau for AgNPs volume of 500-800 μl (i.e. pyrene-AgNPs ratio of 1:5-1:8) at the intensity level of ~1.2 times higher than pure pyrene.

The processes of pyrene fluorescence quenching and enhancement near AgNPs are governed by the electron and energy transfer due to a concentration-dependent separation of pyrene molecules from the AgNPs surface [26], possible AgNPs aggregation [27], and increased fluorescence excitation due to an enhanced electric field near AgNPs [20]. In addition, the dependence of pyrene fluorescence intensity on the AgNPs concentration in Fig. 7 follows the known trend of fluorescence enhancement on the fluorophore-nanoparticle distance with quenching observed at a short distance followed by enhancement at an optimal distance and then slow enhancement decrease with distance increase [4, 19].

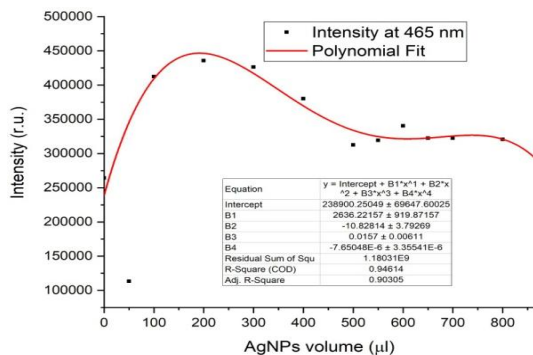


Fig. 7 – Dependence of peak fluorescence intensity at 465 nm on the AgNPs volume in solution containing 100 μl pyrene (symbols) and polynomial approximation (solid line)

3.3 Fluorescence Measurements of Pyrene-Containing Nanocomposite Thin Films with Different AgNPs Concentration

Further studies were conducted to evaluate the influence of AgNPs concentration on the PEF response of pyrene-containing nanocomposite thin films prepared as described in subsections 2.2.3-2.2.4. As it can be seen from Fig. 8, the highest fluorescence intensity (~ 2.1 times higher than pure pyrene) is achieved for the pyrene-AgNPs volume ratio of 1:1. In addition, there is no significant difference in fluorescence intensity in the presence of AgNPs, when pyrene-AgNPs ratios change from 2.5:1 to 1:1. The absence of fluorescence quenching of pyrene and increased PEF efficiency of the nanocomposite thin films containing AgNPs, when compared to pyrene-AgNPs solutions, implies the significant role of the polymer matrix in providing an optimal arrangement of AgNPs and pyrene molecules.

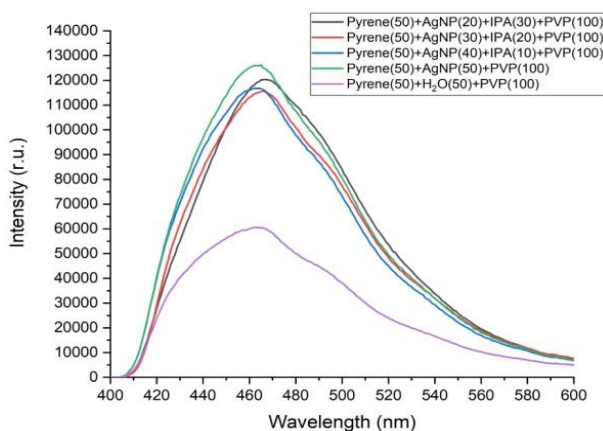


Fig. 8 – Fluorescence spectra of pyrene-containing nanocomposite thin films without AgNPs and with different pyrene-AgNPs volume ratios in the range of 2.5:1 – 1:1. Volumes of solution components in microliters are shown in the legend

4. CONCLUSION

PEF effect for a pyrene-AgNPs system was studied theoretically and experimentally in solutions and nanocomposite thin films depending on the AgNPs concentration. Using FEM modeling in COMSOL it was shown that the distance between AgNPs and fluorophore molecules, as well as the size of the AgNPs, influence the fluorescence emission due to the changes in electric field strength enhancement. Specifically, simulation results demonstrate that the highest PEF efficiency for pyrene molecules can be expected at a distance of up to 5 nm from the surface of AgNPs with a diameter of 20 nm.

The chemically synthesized AgNPs with an average diameter of ~ 20 nm were used to achieve PEF in pyrene-AgNPs solutions and nanocomposite thin films by tuning the AgNPs concentration. It was found that the PEF effect occurs in a broad range of the pyrene-AgNPs volume ratio in solution (1:1-1:8, with a highest enhancement of ~ 1.8 times at 1:2), except for a 2:1 ratio

when fluorescence quenching is observed. In case of a nanocomposite thin film, the highest fluorescence intensity enhancement (~ 2.1 times higher than pure pyrene) was achieved for the pyrene-AgNPs volume ratio of 1:1. Moreover, PEF effect was also observed for pyrene-AgNPs ratios from 2.5:1 to 1:1, which demonstrates the importance of the PVP matrix for an optimal arrangement of AgNPs and pyrene molecules. These results provide new insights into the optimization of

plasmonic nanostructures and their nanocomposites with fluorophores for maximizing the PEF effect for use in photonic and sensing applications.

ACKNOWLEDGEMENTS

This work was supported by the National Research Foundation of Ukraine, project 2023.04/0057.

REFERENCES

1. S.A. Maier, *Plasmonics: Fundamentals and Applications* (Springer US, New York, NY, 2007).
2. K.L. Kelly, E. Coronado, L.L. Zhao, G.C. Schatz, *J. Phys. Chem. B* **107**, 668 (2003).
3. T. Sergeeva, D. Yarynka, V. Lytvyn, P. Demydov, A. Lopatynskiy, Y. Stepanenko, O. Brovko, A. Pinchuk, V. Chegel, *Analyst* **147**, 1135 (2022).
4. A. Lopatynskiy, V. Lytvyn, M. Khutko, A. Pinchuk, V. Chegel, *Sensor. Actuat. A: Phys.* **389**, 116558 (2025).
5. M. Reale, Z. Moussadjy, G. Buscarino, U. De Giovannini, A. Emanuele, M. Cannas, R. Cillari, N. Mauro, A. Sciortino, F. Messina, *Nanoscale* **17**, 9380 (2025).
6. J.R. Lakowicz, *Analytical Biochem.* **337**, 171 (2005).
7. A. Kinkhabwala, Z. Yu, S. Fan, Y. Avlasevich, K. Müllen, W.E. Moerner, *Nat. Photon* **3**, 654 (2009).
8. V.I. Chegel, V.K. Lytvyn, A.M. Lopatynskiy, P.Ye. Shepelyavii, O.S. Lytvyn, Yu.V. Goltvyanskyi, *Semicond. Phys. Quantum Electron. Optoelectron.* **18**, 272 (2015).
9. S. Dasgupta, K. Ray, *Front. Chem.* **12**, 1407561 (2024).
10. G.V. Bünau, *Ber. Bunsenges Phys. Chem.* **74**, 1294 (1970).
11. D. Arumugam, N.A. Jamuna, A. Kamalakshan, S. Mandal, *ACS Appl. Bio Mater.* **7**, 6343 (2024).
12. S. Patel, J. Seet, L. Li, J. Duhamel, *Langmuir* **35**, 13145 (2019).
13. K.G. Thomas, P.V. Kamat, *Acc. Chem. Res.* **36**, 888 (2003).
14. X. Feng, X. Wang, C. Redshaw, B.Z. Tang, *Chem. Soc. Rev.* **52**, 6715 (2023).
15. K. Aslan, I. Gryczynski, J. Malicka, E. Matveeva, J.R. Lakowicz, C.D. Geddes, *Curr. Opinion Biotechnol.* **16**, 55 (2005).
16. E. Dulkeith, A.C. Morteani, T. Niedereichholz, T.A. Klar, J. Feldmann, S.A. Levi, F.C.J.M. Van Veggel, D.N. Reinhoudt, M. Möller, D.I. Gittins, *Phys. Rev. Lett.* **89**, 203002 (2002).
17. D. Lee, J. Song, G. Song, Y. Pang, *Nanoscale Adv.* **4**, 2794 (2022).
18. C.D. Geddes, J.R. Lakowicz, *J. Fluorescence* **12**, 121 (2002).
19. P. Anger, P. Bharadwaj, L. Novotny, *Phys. Rev. Lett.* **96**, 113002 (2006).
20. Y. Zhang, K. Aslan, M.J.R. Previte, C.D. Geddes, *Chem. Phys. Lett.* **458**, 147 (2008).
21. G. Battistini, P.G. Cozzi, J.-P. Jalkanen, M. Montalti, L. Prodi, N. Zaccheroni, F. Zerbetto, *ACS Nano* **2**, 77 (2008).
22. A.M. Lopatynskiy, Y.O. Malymon, V.K. Lytvyn, I.V. Mogylyni, A.E. Rachkov, A.P. Soldatkin, V.I. Chegel, *Plasmonics* **13**, 1659 (2018).
23. V.I. Chegel, O.M. Naum, A.M. Lopatynskiy, V.K. Lytvyn, in *Nanoplasmonics, Nano-Optics, Nanocomposites, and Surface Studies* (Ed. by O. Fesenko, L. Yatsenko), **167** (Springer International Publishing, Cham), 395 (2015).
24. A.M. Lopatynskiy, O.G. Lopatynska, L.J. Guo, V.I. Chegel, *IEEE Sensors J.* **11**, 361 (2011).
25. Q. Ke, L. Chen, B. Fang, Y. Chen, W. Zhang, *Mater. Today Commun.* **26**, 101953 (2021).
26. D.S. Rahman, S. Deb, S.K. Ghosh, *J. Phys. Chem. C* **119**, 27145 (2015).
27. R. Gill, L. Tian, W.R.C. Somerville, E.C. Le Ru, H. Van Amerongen, V. Subramaniam, *J. Phys. Chem. C* **116**, 16687 (2012).

Вплив концентрації наночастинок срібла на плазмон-підсилену флюоресценцію пірену в розчині та тонкій нанокompозитній плівці

П.В. Демидов¹, А.М. Лопатинський^{1,2}, В.В. Кузнецов¹, В.К. Литвин¹, М.М. Хутько¹, В.І. Чегель^{1,2}

¹ Інститут фізики напівпровідників ім. В. С. Лашкарьова НАН України, 03028 Київ, Україна
² Навчально-науковий інститут високіх технологій КНУ імені Тараса Шевченка, 01601 Київ, Україна

У цій роботі досліджується вплив концентрації наночастинок срібла (AgНЧ) на плазмон-підсилену флюоресценцію (ППФ) молекул пірену в розчинах та вбудованих у тонкі нанокompозитні плівки на основі полімерів. Використовуючи числове електромагнітне моделювання для оцінки впливу розміру AgНЧ та відстані між наночастинами та флюорофорами на ефективність ППФ, а також систематично змінюючи концентрацію AgНЧ в експерименті, ми досліджуємо, як їхній локалізований поверхневий плазмонний резонанс модулює інтенсивність флюоресценції та спектральні характеристики пірену у водних розчинах та тонких плівках AgНЧ/пірен/полівінілпіролідон, виготовлених методом спіноатингу. Наші результати демонструють нелінійну залежність між концентрацією AgНЧ та інтенсивністю флюоресценції пірену, з оптимальними об'ємними співвідношеннями пірен-AgНЧ 1:2 та 1:1, які максимізують коефіцієнт підсилення флюоресценції для розчину (~ 1.8 разів) та тонкої плівки нанокompозиту (~ 2.1 разів), відповідно. Обговорюється роль полімерної матриці для максимізації ефекту ППФ та запобігання гасінню флюоресценції. Ці результати поглиблюють розуміння можливості налаштування ППФ у гібридних наноструктурах та підкреслюють важливість фактору концентрації наночастинок у розробці ефективних плазмонних флюоресцентних систем для сенсорних та фотонних застосувань.

Ключові слова: Срібні наноструктури, Пірен, Плазмон-підсиленна флюоресценція, Локалізований поверхневий плазмонний резонанс, Метод скінченних елементів, Нанокompозитні матеріали.